CZECH TECHNICAL UNIVERSITY IN PRAGUE

Faculty of electrical engineering

Department of electromagnetic field

Transmissions of Optical Beams and Radio Waves in Optical Turbulent Channel

Diploma thesis

Study plan: Electronics and Communications

Specialization: Radio and Optical technology

Thesis supervisor: Prof. Ing. Stanislav Zvánovec, Ph.D.

Thesis specialist: Ing. Jan Bohata, Ph.D.

Daniel Dousek

Prague 2019

Entry:

Analyze the impact of turbulence on optical wireless links (Free space optical links, FSO) with different kinds of transmitted signal. Focus mainly on comparison of continuous optical signal and microwave signal, transmitted through optical link as radio over FSO (RoFSO) system. For continuous optical signal specify both theoretically and experimentally the significance of beam deflection and with this related errors for optical communication (beam wandering and pointing error) and further options how to adaptively deflect those beams. In the scope of thesis, experimentally test the impact of turbulence on transmission of continuous optical signal and further also on transmission of microwave signal on optical carrier.

Honorable statement

I declare that I have prepared the project myself with the contribution of the supervisor and I have only used the literature mentioned in the work.

Date: 16th May 2019

……

Signature

Thanks

I would like to thank my supervisor, Prof. Ing. Stanislav Zvánovec, Ph.D., for his great patience and willing help with this thesis; my consultant specialist, Ing. Jan Bohata, Ph.D., for all the help with experiments and simulations; my friend and workmate, Ing. Dong Nhat, for all the cooperation during experiments; and my family for their extensive support during my studies.

Abstract

The goal of this thesis is to analyze how Free Space Optical links are they affected by turbulent environment. It is focused on two types of singal: continuous wave and microwave signal on optical carrier known as Radio over Free Space Optics. Both of these signals are then experimentally measured and described including the turbulence errors such as beam wandering and pointing error.

Keywords

Free Space Optics, beam wandering, pointing error, Radio over FSO, turbulence

List of contents

1 Introduction

Atmosphere is not homogeneous and is affected by temperature, pressure and small objects in form of water molecules and the air itself. These fluctuations affect propagating optical wave in different manners depending on the size of fluctuations compared to the beam diameter, wavelength and other. The behavior of optical wave has to be taken into account when designing laser radars, adaptive optics, laser designation and other optical systems [1].

Increasing need for quality high data rate wireless networks has led for several technologies to emerge from research laboratories. Free Space Optics (FSO) is one of them. It presents high bit rate links outside of licensed spectrum with other advantages. It comes with disadvatage in form of unpredictable scintillations as metioned above. These scintillations create unwanted phenomena known as turbulence, observed as beam wandering [2]. Because of narrow optical beam, misalignemt (pointing error) is another subject for future improvement [3].

Chapter 2 will provide theoretical background for atmospheric effects such as absorption, scattering and turbulence. It will also talk about refractive index structure parameter and beam wandering. Chapter 3 is dedicated to pointing error. Then in chapter 4 we will talk about FSO applications and active tracking of receivers. Chapter 5 provides information about RoFSO systems. Simulations will be covered in chapter 6. Chapter 7 is focused on measurments of FSO and RoFSO links. Then chapter 8 provides results for the measurments and lastly chapter 9 is conclusion of whole work.

2 Atmospheric effects

FSO communication systems are of two main types, terrestrial and Earth to space. Terrestrial communication links are affected only by near Earth troposphere and refractive index structure parameter C_n^2 (chapter 2.4.1) can be considered as constant. On the other hand Earth to space links are more complex because C_n^2 differs with altitude. Both links are affected the most by troposphere due to highest density of molecules and changing weather compared to higher atmosphere layers. The most noticeable effects affecting the beam propagation are absorption, scattering, refraction and thermal turbulence [2, 4, 5].

2.1 Absorption

Atmospheric absorption decreases the amplitude of signal due to interaction of light with molecules of the medium, through which it propagates. The extent of absorption is affected by local temperature, pressure, composition of air and mainly by the wavelength of the beam itself. In Figure 1 we can see dependence of wavelength on absorption. Atmosphere is opaque for signal wavelengths between 30 μm and 300 μm. On shorter wavelengths we can see really low absorption with only few high absorption regions [2, 4].

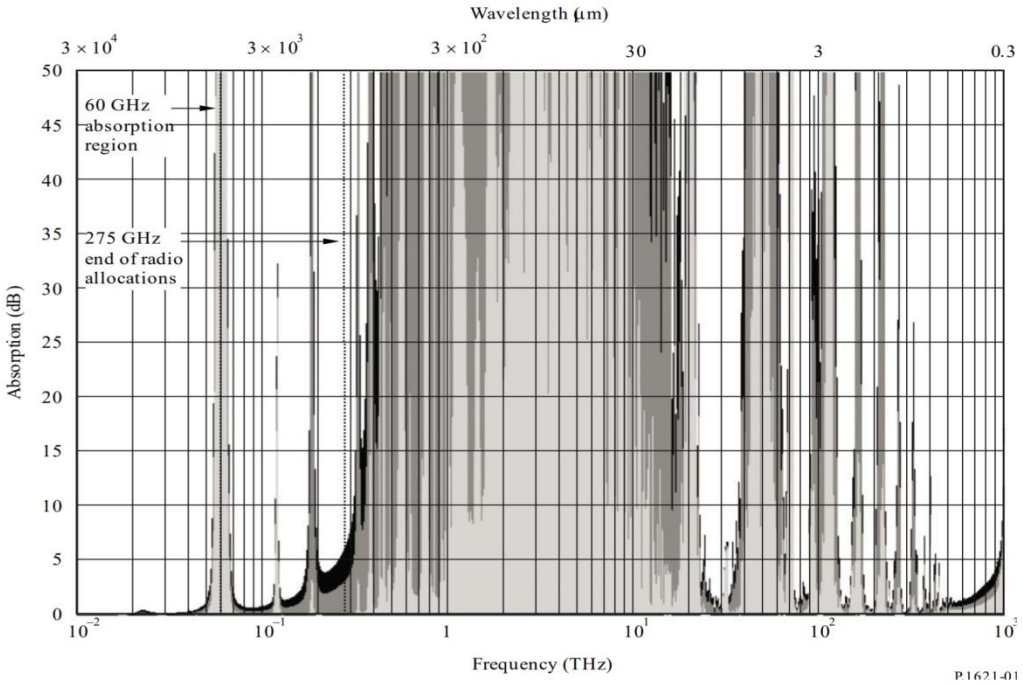

Figure 1 - Graph showing dependence of absorption on wavelength [2]

2.2 Scattering

Atmospheric scattering happens on every molecule or atom and causes part of energy to change its direction of propagation, resulting in decrease of signal strength. The type of scattering depends on diameter of the particle. We can split up these types into two most significant [2]:

- Rayleigh scattering manifests when particle diameter along the propagation line is much lower than wavelength of the electromagnetic wave. This scattering is negligible for wavelengths above 0.8 µm. Below this wavelength raises a lot with dependence of λ^{-4} [2]. Apart from loss in signal strength, scattering of sunlight creates additional noise on receivers, but is negligible during night [4].
- On the other hand, Mie scattering is caused by particles of similar diameter as the wavelength for wavelengths between 0.8 µm and 15 µm. Dominant are microscopic water particles such as fog or mist and the attenuation is much higher for these wavelengths than caused by Rayleigh scattering as shown in Figure 2 [2].

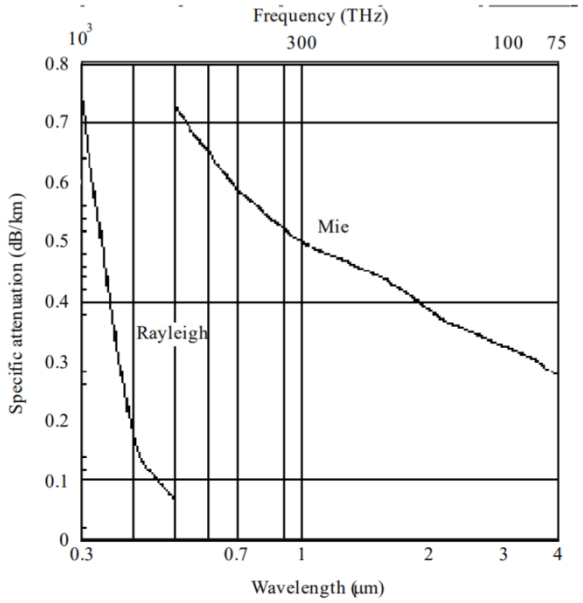

Figure 2 - Comparison of specific attenuations of Mie and Rayleigh scatterings [2]

2.3 Refraction

Atmospheric refraction occurs due to different densities of media along the propagation path. Affected wave changes its propagation path. This affects mainly Earth-Space communication links. It depends primarily on wavelength and elevation angle but also on temperature and pressure. We can calculate atmospheric refractive index n_{eff} for wavelengths below 2 μm by following ITU-R P.1621-2 recommendation [4]. We can predict the true elevation angle Θ_t to the spacecraft by applying the Snell's law and using the n_{eff} from above in the equation (1) [2]

$$\Theta_{obs} = \cos^{-1}\left(\frac{\cos(\Theta_t)}{n_{eff}(T,P)}\right), \quad (1)$$

where Θ_{obs} is observed elevation angle.

2.4 Turbulence

Thermal turbulences create cells of different temperature than the rest of medium. These turbulent cells size from millimeters to tens of meters and have different refractive indices [2, 4, 5]. Small cells cause scattering and multi-paths which reflect in small but quick fluctuations of amplitude on receiver side and overall beam widening as depicted in Figure 3 [5].

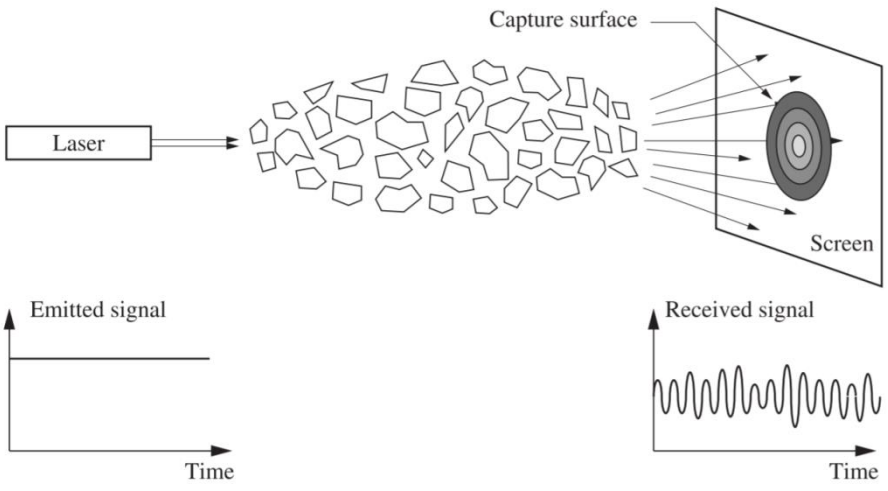

Figure 3 - Deviation of beam in small cell turbulence [5]

On the other hand large cells result in deviation of signal path and can be observed as sizeable but slower fluctuations of amplitude on receiver side as shown in Figure 4 [5].

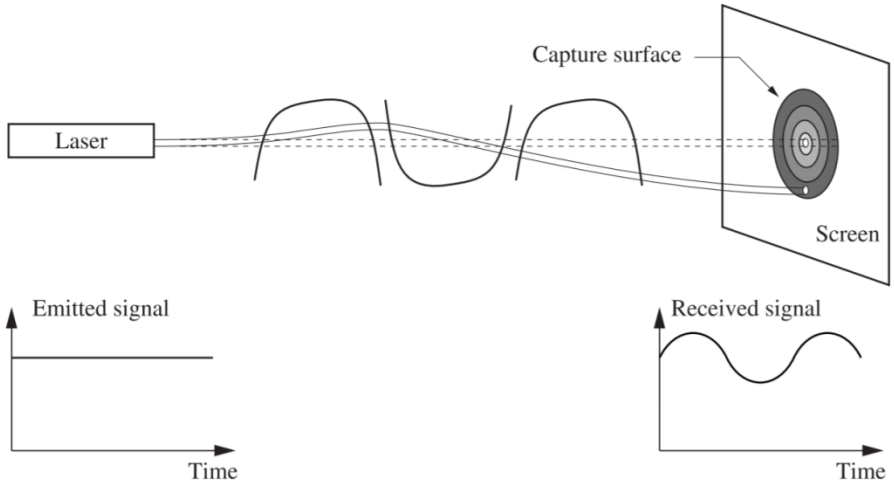

Figure 4 - Deviation of beam in large cell turbulence [5]

When the medium contains both small and large cells we call it scintillation and it is basically sum of the two phenomena mentioned above.

2.4.1 Refractive index structure parameter C_n^2

It is height dependent measure of strength of atmospheric turbulence with unit of $m^{-2/3}$. It depends on local nominal value of surface turbulence C_0 (typically 1.7×10^{-14} $m^{-2/3}$), ground wind speed v_g (typically 2.3 m/s) and height above ground level h (m). We can calculate C_n^2 as (3) [2]

$$C_n^2(h) = 8.148 \times 10^{-56} v_{rms}^2 h^{10} \exp^{-\frac{h}{1000}} + 2.7 \times 10^{-16} \exp^{-h/1500} + C_0 \exp^{-h/100} \quad (2)$$

where v_{rms} is calculated as (2) [2]

$$v_{rms} = \sqrt{v_g^2 + 33.11 v_g + 360.31} \quad (3)$$

For horizontal communication link, C_n^2 is constant, but for vertical link, the calculation leads on integral with increasing step h_i as shown in (4)

$$h_i = \exp\left\{\frac{i-1}{20}\right\} \qquad \text{m} \tag{4}$$

where $i = 1$ to 139 [2].

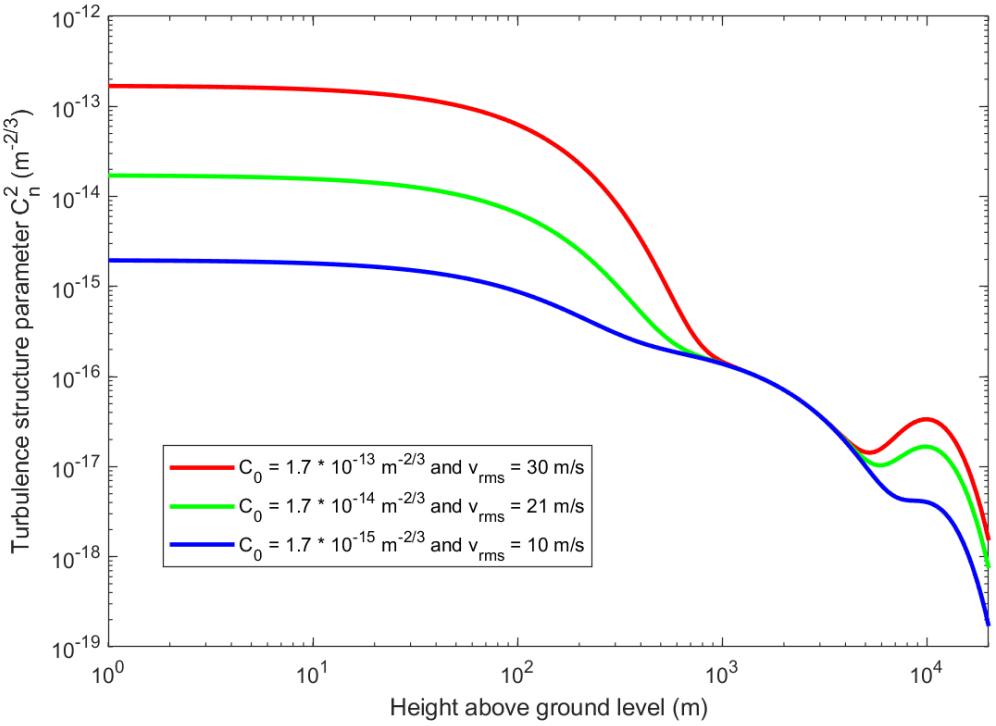

Figure 5 – Refractive index structure parameter as a function of height for several values of surface turbulence and wind speed

Figure 5 shows the dependence of refractive index structure parameter on root mean square ground wind speed v_{rms} and nominal surface turbulence C_0 for different heights ranging from 0 m to 20 km. It indicates that for first 100 m from ground, the function is close to constant and depends only on surface turbulence. On the following part of graph till 4 000 m, the refractive index structure parameter starts to gradually drop and for the last 16 000 meters it is highly dependent on ground wind speed.

2.4.2 Atmospheric coherence length r_0

This parameter describes the effective aperture of receiver. If the receiver is larger than optimum, it receives degraded waveform. It is dependent on wavelength λ, zenith angle ξ and refractive index structure parameter C_n^2. Equation 5 shows the calculation of coherence length r_0 (5) [2]

$$r_0 = \left(0.423(2\pi/\lambda)^2 \sec\xi \int_{h_0}^{Z} C_n^2(h)\mathrm{d}h\right)^{-3/5}, \quad (5)$$

where h is height above ground level and Z is effective height of turbulence (20 000 m).

2.5 Beam Wander

Beam wander is significant in Earth to Space direction and negligible in Space to Earth direction links, as it propagates through the turbulent are only for few last kilometers. It is direct impact of large turbulence cells and describes the displacement of the beam from the point of maximum irradiance during time (Figure 6). When the displacement is high, receiver receives skewed Gaussian beam. The following equation (6) shows root mean square displacement of wandering beam σ_{rc}: [5, 6]

$$\sigma_{rc} = 2080 \cdot L \sqrt{\frac{\int_{h_0}^{Z} C_n^2(h)\mathrm{d}h}{D_T^{1/3}\sin\theta}}, \quad (6)$$

where L is propagation distance, D_T is diameter of the transmitting aperture, h is height above ground level and Z is effective height of turbulence (typically 20 000 m).

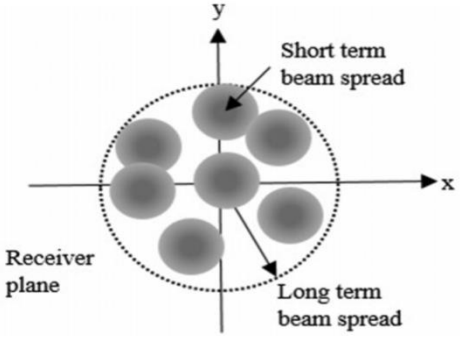

Figure 6 - Beam Wandering [7]

Figure 6 shows “wandering” of the beam spot on the receiver plane during time.

Figure 7 are theoretical calculations for beam wandering in the height above ground of 30 meters, laser beam half-width of 14 mm and horizontal propagation path. It is clearly visible that beam wandering limits high turbulent areas for horizontal links longer than 1 km for small lenses below 1 cm in diameter.

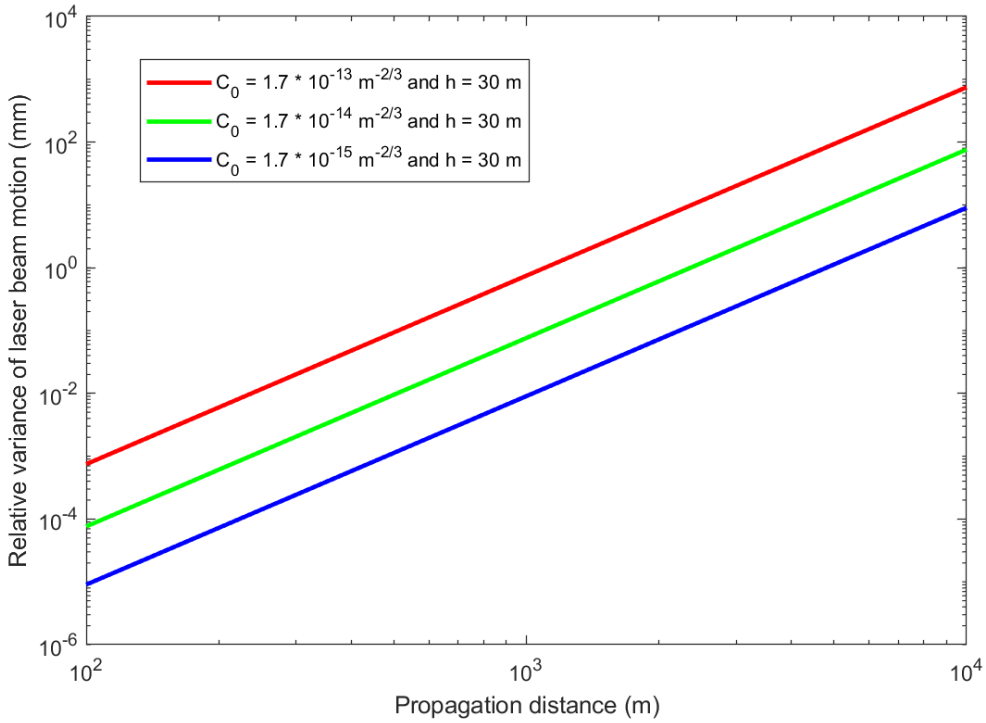

Figure 7 - Relative variance of laser beam motion during horizontal propagation path in height of 30 m

3 Pointing error

Free Space Optic communication links are affected by atmospheric effects such as turbulence and absorption. But they are also affected by accuracy of pointing of the beam on the receiver. Pointing error appears when there is mechanical misalignment of transmitter and receiver. When link is established, it has fixed pointing error and small jitter error in the form of small vibrations [5]. Misalignment losses can be calculated as [8]

$$A_{PE} = \left|10 \log \frac{P_1}{P_0}\right|, \qquad [\#]$$

where P_1 is power received by misalignment and P_0 is power received by perfect alignment. These losses depend on the beam optical power intensity distribution. Most common is Gaussian, but other distributions can decrease the impact of pointing error. Another way to increase performance is larger lenses, which would catch whole beam spot even during misalignment. Figure 8 depicts how misalignment decreases received power for Gaussian beam.

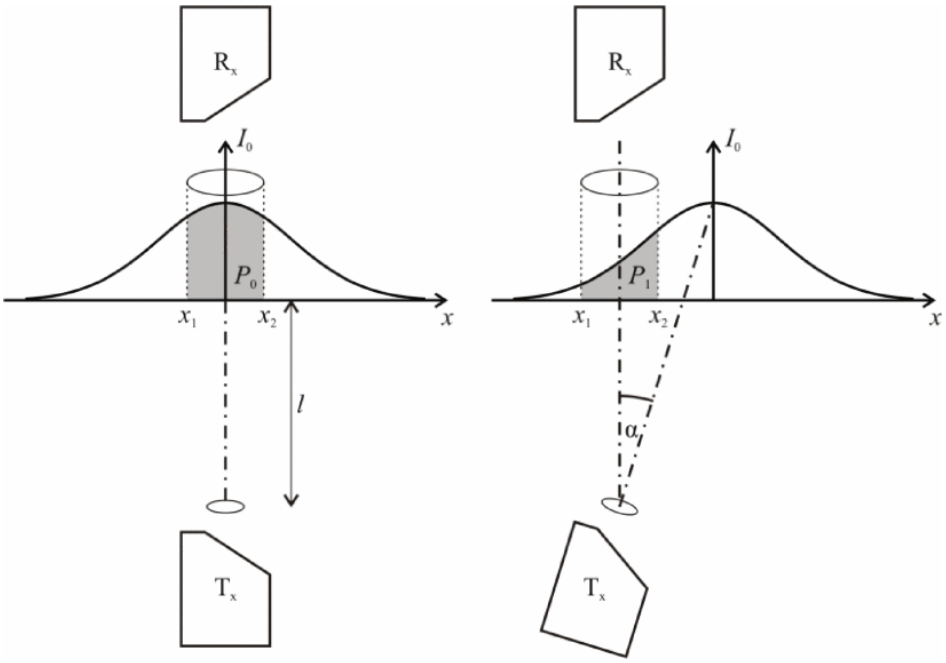

Figure 8 – Pointing error received power for Gaussian beam [8]

4 Adaptive beam deflection and usage for FSO

Free Space Optics link is designed to be point-to-point because laser does not spread as radio wave does. This secures the link from tapping, but makes it much harder to realize communication link between moving stations. First problem is pointing error itself and also the problem of computing and predicting the flight path of moving station for on go real time adjustment. Another problem is in the form of large cell turbulences which cannot be predicted and they have to be compensated by real time tracking of changes in the atmosphere [9].

Figure 9 shows example of communication between Earth station and satellite. Satellite at point R1 sends signal towards Earth, which receives it under some angle θ and by that time satellite changes position to R2. Earth station has to compensate both the movement from R1 to R2, but also adjust for the time until the signal reaches the satellite at point 3 by adding θ_L in radians to θ. Angle θ_L can be calculated with simplified expression (7)

$$\theta_L = \frac{2(v_S - v_E)}{c}, \tag{7}$$

where v_S is tangential velocity of the satellite, v_E is tangential velocity of the Earth station and c is speed of light. [5]

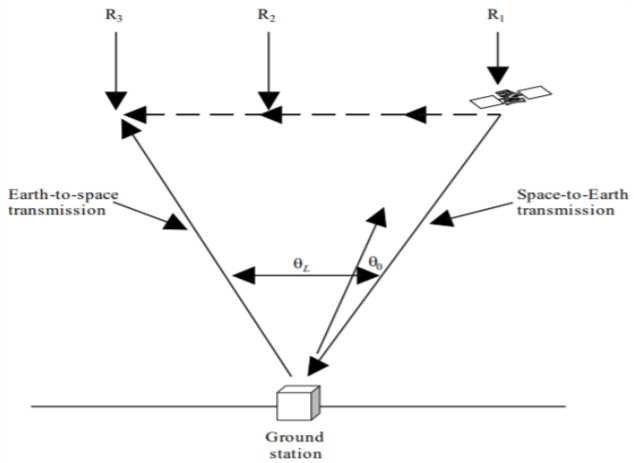

Figure 9 - Compensation for satellite movement [5]

FSO has various applications such as Earth to satellite connection, last mile access [11], enterprise connections [12], fiber backup or military usage due to high link security which is hard to intercept [13]. Between other advantages belong communication range, license-free operation and very high speed data rate. Limitations are scintillations and necessity for obstacle free path.

Because 1550 nm FSO link does not convert optical to electrical and vice versa, need for reconfiguration of transmitter disappears even when we change data rate, signal format or optical wavelength within nanometers. System based on this configuration is reaching data rates of up to 1TB/s [14].

We need to counter atmospheric turbulence or building sway because optical beam is narrow and misalignment would lead to high losses in optical power, therefore active tracking is necessary. Usage of signal beacon and quadrant photo detector has been reported in [14]. System can actively analyze and counter beam wandering by real time adjustments keeping most of the optical power focused onto a core of SMF-28 fiber.

Other usage of FSO is indoors, where atmospheric turbulences are not present. These links are implemented in places, where it is difficult to use wired transmission. Line-of-sight, tracked or diffused transmission configurations are in use [14].

Air-to-air and air-to-ground systems for military usage are presented in [15]. They propose spherical receivers for easier reception of signal from moving objects such as military unmanned aerial vehicles, where very high data rate and channel security is very important aspect.

5 Radio over FSO

FSO is using optical wave as medium to transfer information from point A to point B, how to adjust it to carry more and more data has been studied for many years. Starting with simple signaling with a lamp using Morse code has been used over 100 years ago. In present world we needed something faster, something that can compete with conventional radio frequency transmission and metallic cables, while staying affordable and compatible with already existing systems. We started modulating lasers. Easiest way was to turn the laser on and off, where on would represent binary 1 and off would be 0. This method became conventional under the name of On-Off-Keying (OOK). Both non-return-zero (NRZ) and return-zero (RZ) line codes are in use, where NRZ. OOK is currently dominant in the world due to its simplicity and resistance to laser nonlinearities [16].

Between other options comes the use of radio frequency (RF) data signal applied on optical carrier also known as Radio over FSO (RoFSO) [11] or Radio over Fiber (RoF) for directly compatible fiber usage. This is mostly in experimental usage and takes advantages of two regions: easy to generate RF signal and noise resistant optical signal. This would enable high speed wireless links in areas where laying down cables or setting up satellites would be more costly than FSO link or just for temporary high speed links. Proposed scenario is in Figure 10. The most common wavelengths are 850 nm and 1550 nm [14] as they reflect telecommunication window of fiber optics. RoFSO can employ commonly know modulations ranging from Binary Phase Shift Keying (BPSK) to 64-Quadrature Amplitude Modulation (64-QAM) and many others [17].

Figure 10 - Example of RoF and RoFSO scenario [12]

Another advantage is simple setup: laser diode with Mach-Zehnder modulator (MZM) [18] and a collimator as seen in Figure 11 a). Receiver consists of collimator and detector, for example PIN diode. Other option is to directly modulate a distributed feedback laser [11] as seen in Figure 11 b).

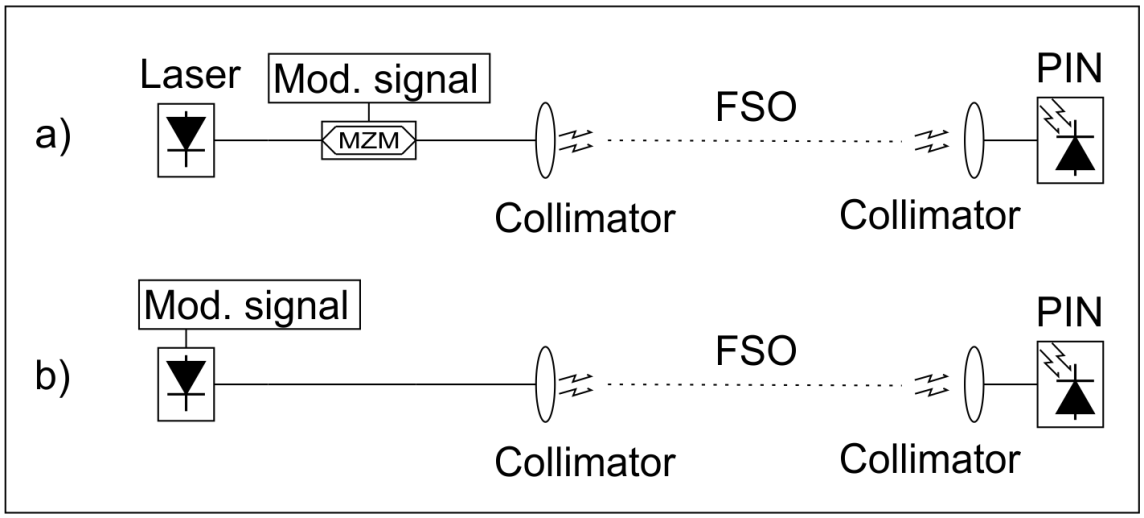

Figure 11 – a) RoFSO MZM modulation; b) RoFSO DFB direct modulation

Compared to metallic and radio transmission, RoFSO provides low attenuation losses, direct compatibility with radio over fiber (ROF), broad bandwidth and immunity to radio interference.

Disadvantage is limited bandwidth for low attenuation windows and limited power transmitted through the air due to possibility of eyesight or even skin damage [16]. Power limitation leads to lower modulations which ultimately mean lower data rates.

We are using RoFSO in chapter 7.3 and 7.4 experiments. In the experiment we are using frequency doubling, but frequency quadrupling [19] using cascade of two symmetrically biased MZMs or eightfold [20] using only one single-drive MZM has been reported. In our experiment we are using MZM to create optical carrier. Depending on voltage provided to MZM, we can bias how the optical signal looks like in relation to electrical signal. Power transfer function of MZM has three main points where we can place our bias voltage. Most common is Quadrature point, where modulator offers highest linearity. Peak point is where frequency doubling occurs, but optical carrier is not suppressed as opposed, when we place our bias at Null point.

6 Simulations

As we had limited space and tools to conduct our measurements (mainly under turbulence), we simulated some parameters in Optiwave OptiSystem 12.

First interesting value to measure was pointing error: we wanted to know, how transmitter angular misalignment affects received power. Our stages had insufficient angular hatch mark resolution, so we simulated in OptiSystem.

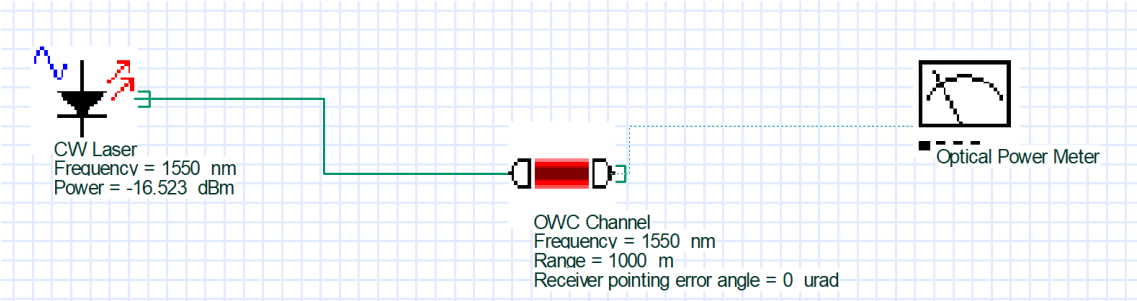

Figure 12 – Schematic block from OptiSystem

We set link length to 40 meters as in later measurement. Input power was set to give us 0 dBm on receiver for 0 µrad error. Simulation result is shown in Figure 13. We can see that received power is exponentially decreasing with angular error reaching almost 1 dB loss for 10 µrad for 2.3 cm lenses.

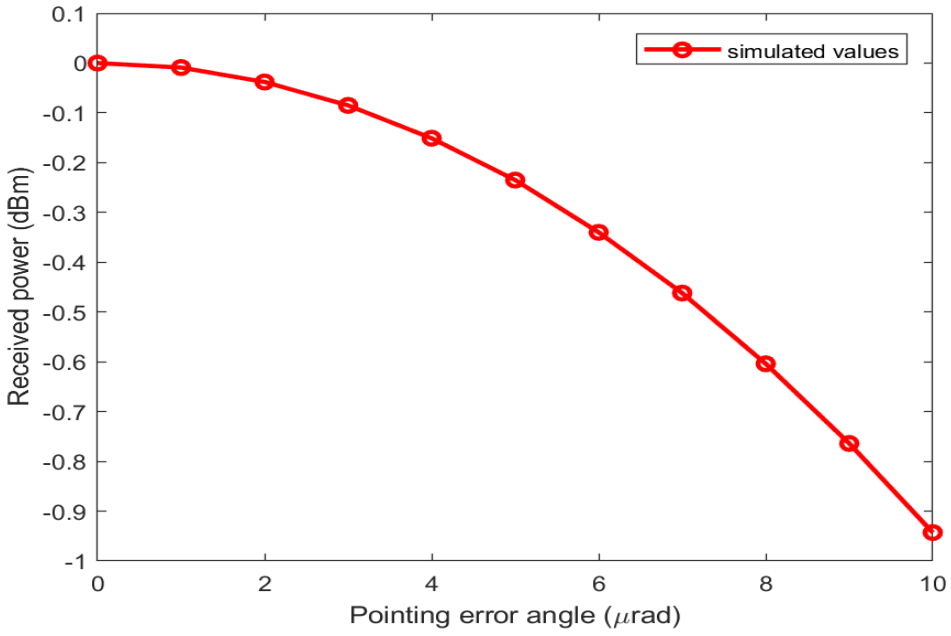

Figure 13 – Dependency of pointing error angle on received power for 40 m FSO link

Next simulated dependency was received power on refractive index structure parameter as seen in Figure 14. Simulations had both 40 m and 1 km FSO link length. Additional loss difference between low and high turbulence was less than 0.4 dB for 40 m link and almost 7 dB for 1 km link. It must be noted that this simulation had no pointing error. Also worth mentioning is 16.5 dB loss of the channel with no turbulence which is 4 dB worse than what we achieved in chapter 7.4 and 8.4. Schematic block for both simulations is shown in Figure 12.

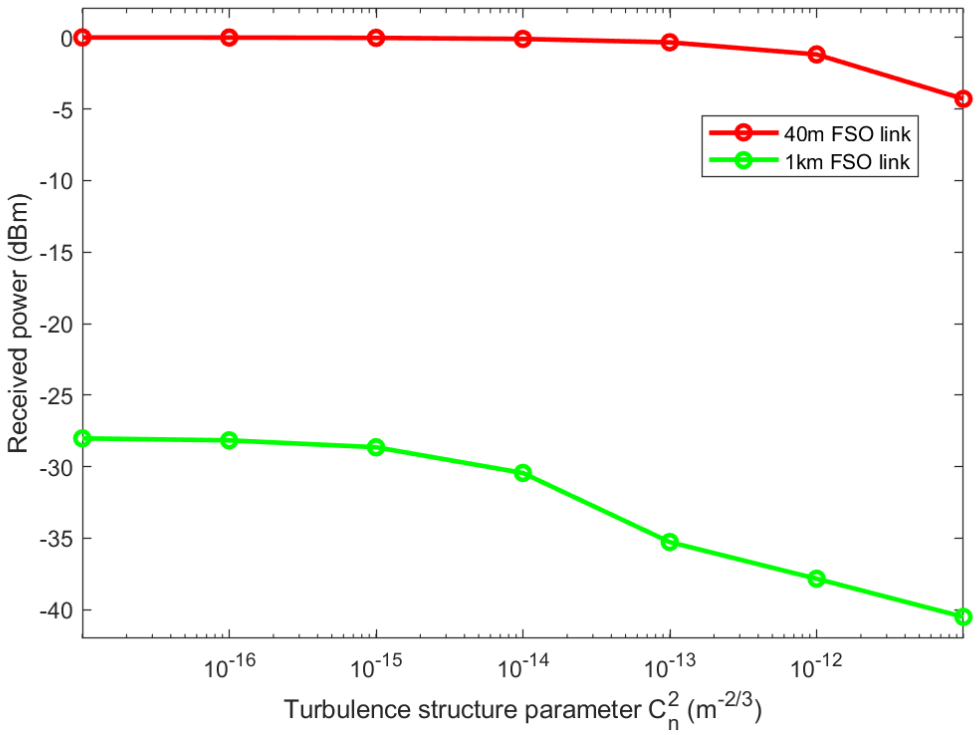

Figure 14 - Dependency of received power on turbulence for 40 m and 1 km FSO link

7 Measurements

In this work we measured various signals and modulations and analyzed how they are affected by different turbulent environments. Every measurement was established in the university campus of the Czech Technical University in Prague. In all schematic blocks are lines connecting each element, those lines are representing approximately 20 centimeters of SMF-28 optical fiber.

In **Continuous wave transmission** (chapters 7.1 and 8.1)**,** we started by constructing simple point-to-point link in non turbulent environment to test our ability of creating stable transmission of a continuous wave laser signal without any data.

In **Turbulence influence on part of FSO** (chapters 7.2 and 8.2), we built an environment for generation of turbulences with ability to measure them and also performed first data transfer with BER tester for fiber optics.

In **RoFSO laboratory tests** (chapters 7.2 and 8.2)**,** we set up complex system for RoFSO consisting of multiple stages: signal generation, FSO link under turbulence, fiber section with EDFA amplifier, point to point microwave link using antennas, and signal evaluation.

In **Long RoFSO test in corridor** (chapters 7.2 and 8.2)**,** we tested longer distance link with similar setup as in previous section, but without any turbulence.

7.1 Continuous wave transmission

First experiment was established as 2 m point-to-point FSO link on optical table, where signal of 1550 nm continuous wave laser from IDPHOTONICS CoBrite DX4 was set to output power of 6dBm. Signal was transmitted through FC/APC connector into 20 cm SMF-28 optical fiber. End of fiber was connected to F810APC-1550 air-space doublet collimator. The collimator was fixed in a mount to both 2-axis angle stage and 3-axis linear stage for precise alignment. Then 2 meters of free space followed, ended with the same combination of collimator and optical fiber with Thorlabs digital handheld optical power meter PM100D attached. As beam was really hard to spot even on detector card of corresponding wavelength, it was necessary to do rough estimate of angle axis at both receiver and transmitter side using red visible laser and then switch to 1550 nm laser with power meter on receiver side for precise tuning. During tuning, we could observe how

much did linear and angle tuning affect received power. Where linear x, y and z axis alignment had almost no effect and had flat peak tune, angular alignment made significant changes on both receiver and transceiver side. Schematic for this experiment is shown in Figure 15.

Figure 15 – Schematic block for continuous wave transmission

7.2 Turbulence influence on part of FSO

For measurement of the communication link in turbulent environment, we built enclosed turbulence chamber with evenly distributed temperature sensors [21, 22].

External air ventilation with ability to change temperature of the air inside the chamber was set up on outer wall. Those ventilators were able to blow air through holes on the side wall to create turbulent environment, which was then processed by MATLAB script.

Rytov variance and refractive index structure parameter is used to describe the strength of turbulences along the propagation path L. The signal fluctuations are characterized by Rytov variance given by [11]

$$\sigma_R^2 = 1.23 k^{\frac{7}{6}} C_n^2 L_6^{11}, \quad (8)$$

where $k = 2\pi/\lambda$ is the wave number and λ is carrier wavelength.

Refractive index structure parameter C_n^2 used to characterize the turbulences is given by

$$C_n^2 = \left(79 \times 10^{-6} \frac{P_a}{T^2}\right)^2 C_T^2, \quad (8)$$

where P_a is the atmospheric pressure in millibars, T is average temperature in Kelvins and C_T^2 is the temperature structure constant defined as

$$C_T^2 = (T_1 - T_2)^2 / L_p^{2/3}, \quad (10)$$

where T_1 and T_2 are temperatures at two points with distance of L_p. Because we had 20 sensors divided by 10 cm spaces, the script computes C_n^2 for each pair of sensor (sensor 1&2; sensor 2&3; sensor 3&4; etc.) as seen in Figure 16, and then gives us average C_n^2 across whole path as final number together with Rytov variance.

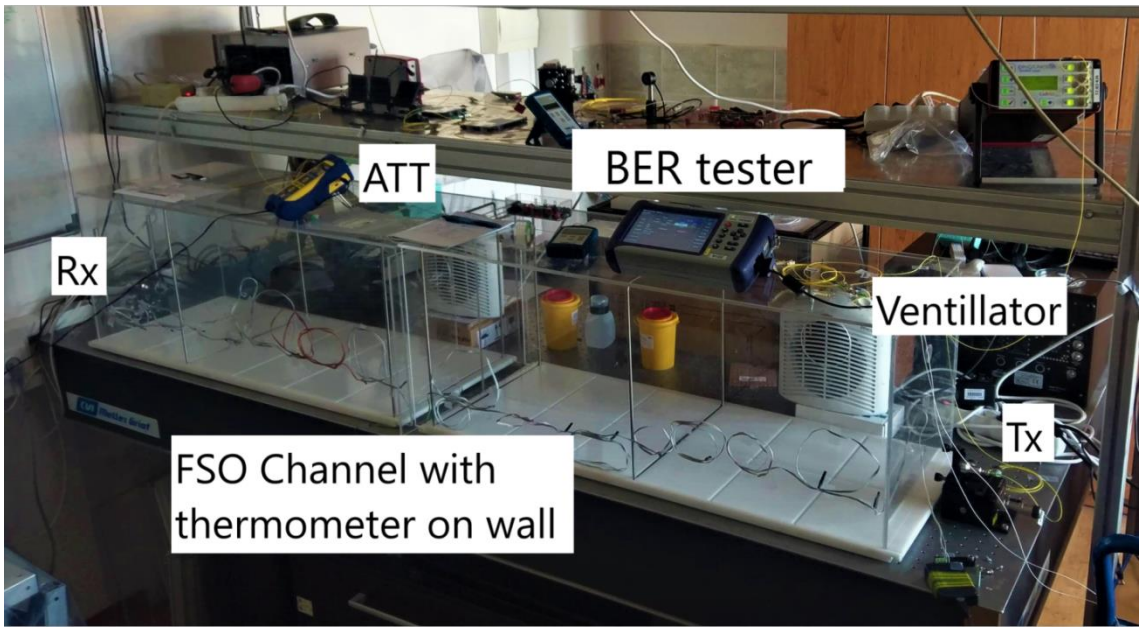

Figure 16 – Picture of setup for continuous wave measurement

After setting up PC with MATLAB script and calibrating our sensors we connected VeEX – VePAL CX350s BER tester into our setup from Continuous wave transmission, where it replaced CoBrite DX4 as input and digital power meter as output. BER tester sends and receives data sequence through SC/AP connectors which were then connected to our setup as seen in Figure 17.

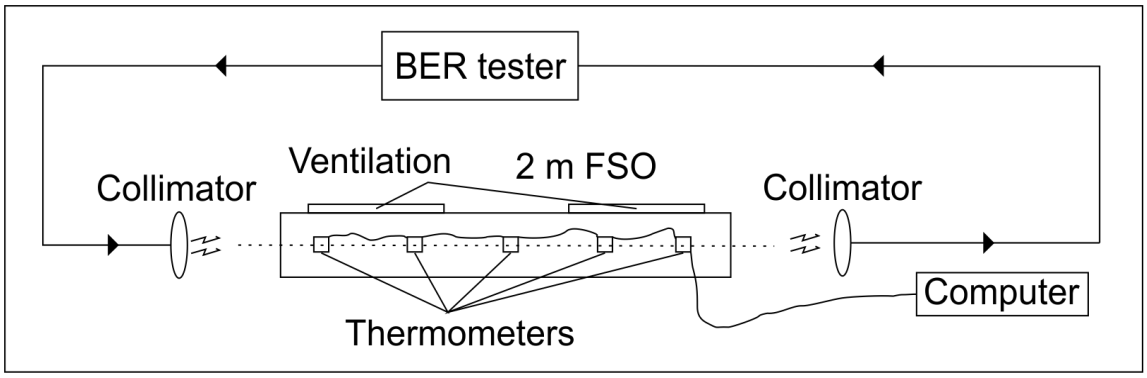

Figure 17 – Schematic block for Turbulence influence on part of FSO

BER tester then sent signal with power level of 1.6 dBm through our optical link and compare transmitted and received bit sequence to compute desired bit error ratio as:

$$BER = \frac{error\ bits}{total\ amount\ of\ trasmitted\ bits} \tag{11}$$

After first run under turbulence no error bits were received as seen in Figure 18, so we added optical attenuator into our setup between Rx of FSO and BER tester input. With few tests, we have decided to set 6 dB of additional attenuation. This corresponded to state, where we can see errors, but not decrease optical power level of signal below detectable level of BER tester for highest achievable turbulence level.

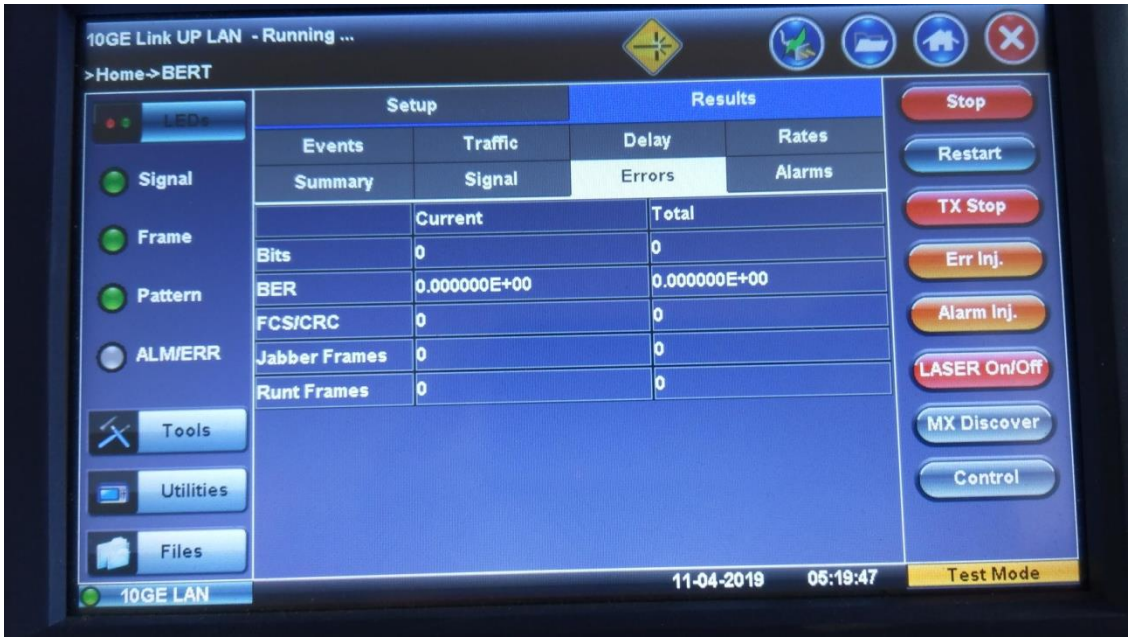

Figure 18 – BER tester user interface showing no errors

7.3 RoFSO laboratory tests

In this section we prepared measurement for RoFSO. As RoFSO is mainly considered to be part of the last mile access, we have decided to simulate, how will the whole anticipated system work, so we added section of optical fiber, EDFA amplifier and microwave wireless link with antennas [23, 24, 25].

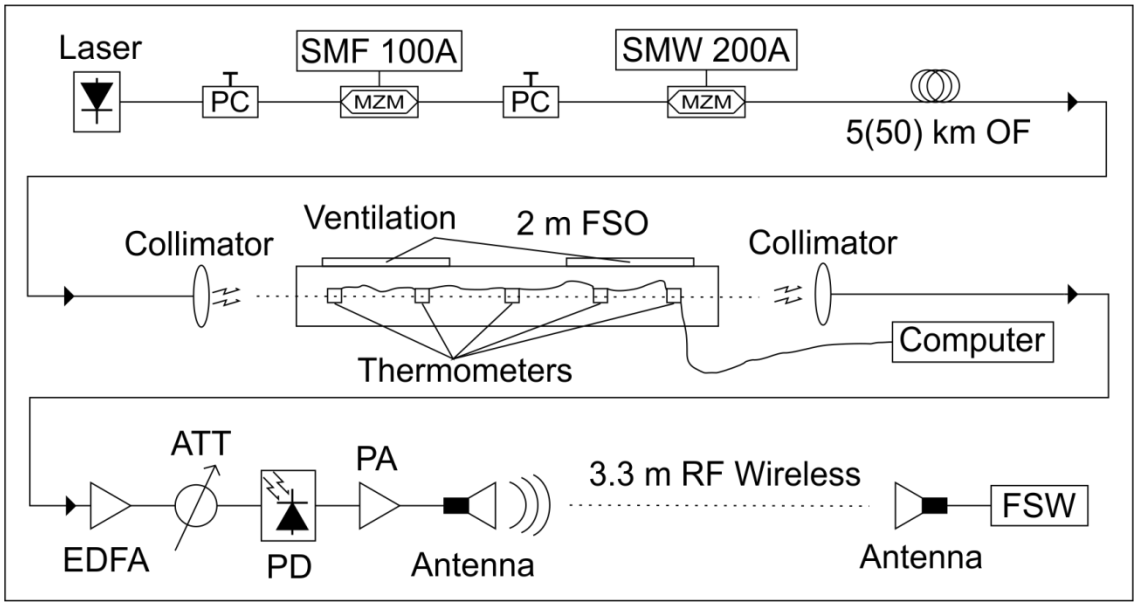

Figure 19 – Schematic block for RoFSO laboratory tests

In Figure 19, we can see our setup for measuring of RoFSO. Laser used as optical signal was generated from IDPHOTONICS CoBrite DX4 with wavelength 1550 nm and 6 dB power output. Signal then went through cascade of two Mach-Zehnder modulators Thorlabs LN81S and two polarization controllers (PC), one before each of the MZMs. First MZM was modulated by R&S SMF100A microwave signal generator with frequency of 12.5 GHz with bias at lowest point (3.4 V) to create our desired suppressed optical carrier [26, 27] with frequency doubling, second MZM was modulated by R&S SMW200A vector signal generator where we set LTE-A test model and 3 different modulation schemes: 4-QAM, 16-QAM and 64-QAM. Modulators were then followed by section of 5 km of optical fiber SMF-28, ended with FSO link from Turbulence influence on part of FSO.

Spectrum of signal is in Figure 20 below, which was separated from our whole setup by 99/1 coupler and visualized on 1% gate by Yokogawa AQ6370C optical spectrum analyzer. We can see our data as the 2 highest peaks around our suppressed optical carrier in the middle.

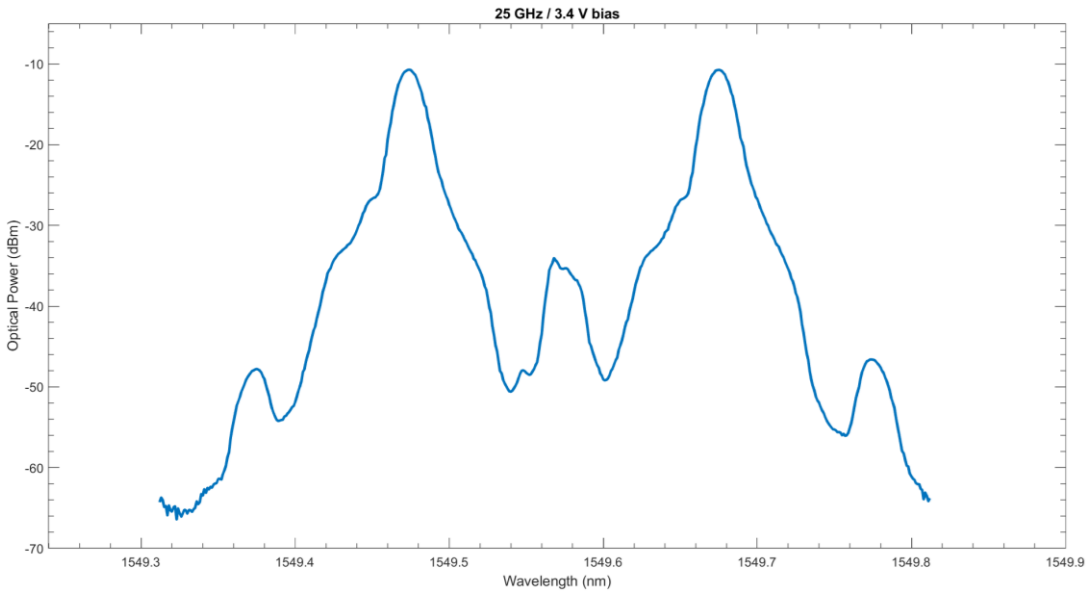

Figure 20 – Optical suppressed carrier signal spectrum

FSO link was followed by erbium doped fiber amplifier (EDFA) Keopsys KPS-BT2-C-10-LN-SA, which amplified our signal by 9.25 dB. After EDFA was placed optical power attenuator for possibility of measuring different optical powers without affecting our optical carrier. This was followed by optical photodetector Optilab PD-40 which converted optical signal into microwave region. Preamplifier Analog devices HMC1131 followed before the microwave signal entered RF channel length of 3.3 meters using two double rigged waveguide horn antennas RFspin DRH40 with transmit power of 4 dBm. At the end of channel R&S FSW signal and spectrum analyzer was used to evaluate the signal.

7.4 Long RoFSO test in corridor

In the last measurement, we wanted to test, if we are able to create our link on longer distance while placing FSO transceiver and receiver on non-stabilized places prone to small vibrations and floor slanting. The corridor in the university building seemed like a promising place, as taking all our laboratory equipment outside would be fairly difficult and random bystanders would be harder to control, not to go right into beam propagation path. Setup was identical to RoFSO laboratory tests, but both FSO and RF link were across the whole hallway without turbulences, which measured 40 meters. We placed both transceiver and receiver on small optical panels and rested them on cupboards with other necessary

equipment such as EDFA, attenuators and power meters. We also tested both 5 and 50 kilometers of optical fiber. Schematic diagram is shown in Figure 21.

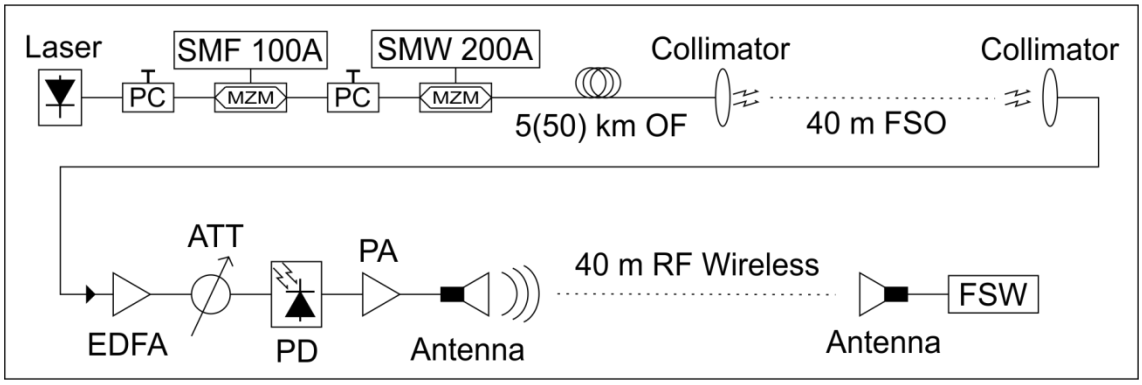

Figure 21 – Schematic block for Long RoFSO test in corridor

In Figure 22 is depicted a view from FSO transmitter; in the background we can see the receiver cupboard. All the equipment for signal generation and evaluation was placed inside of our laboratory to the left.

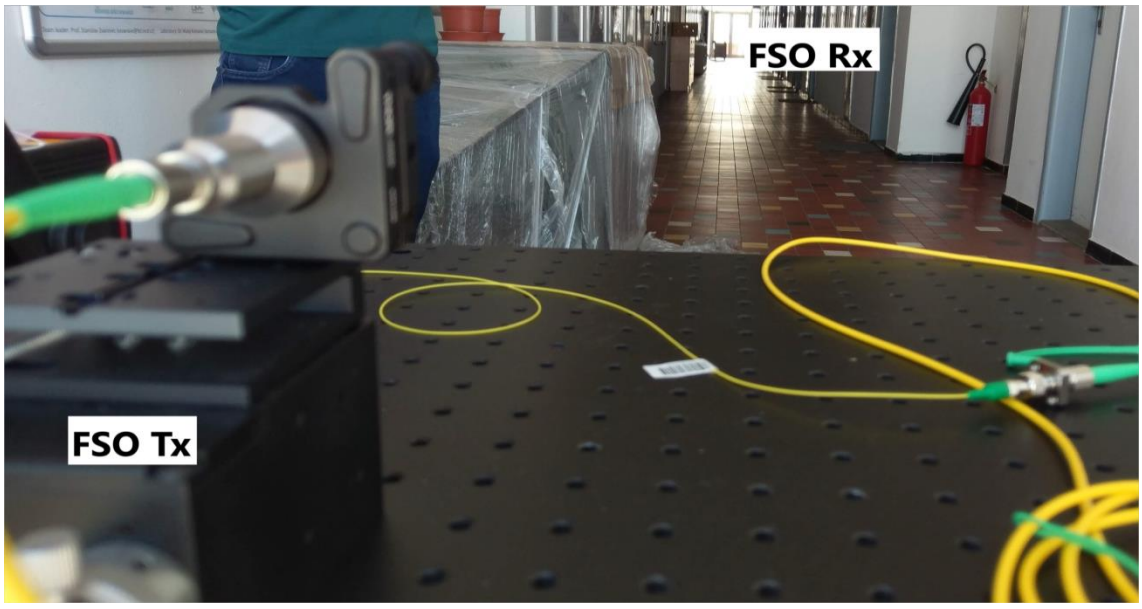

Figure 22 – View of corridor for 40 m FSO link

On the FSO receiver side had to be our EDFA amplifier, attenuator, microwave pre-amplifier, 99/1 coupler with power meter on 1% gate and photodetector with output connected to antenna of microwave link placed on tripod. All these can be seen in Figure 23.

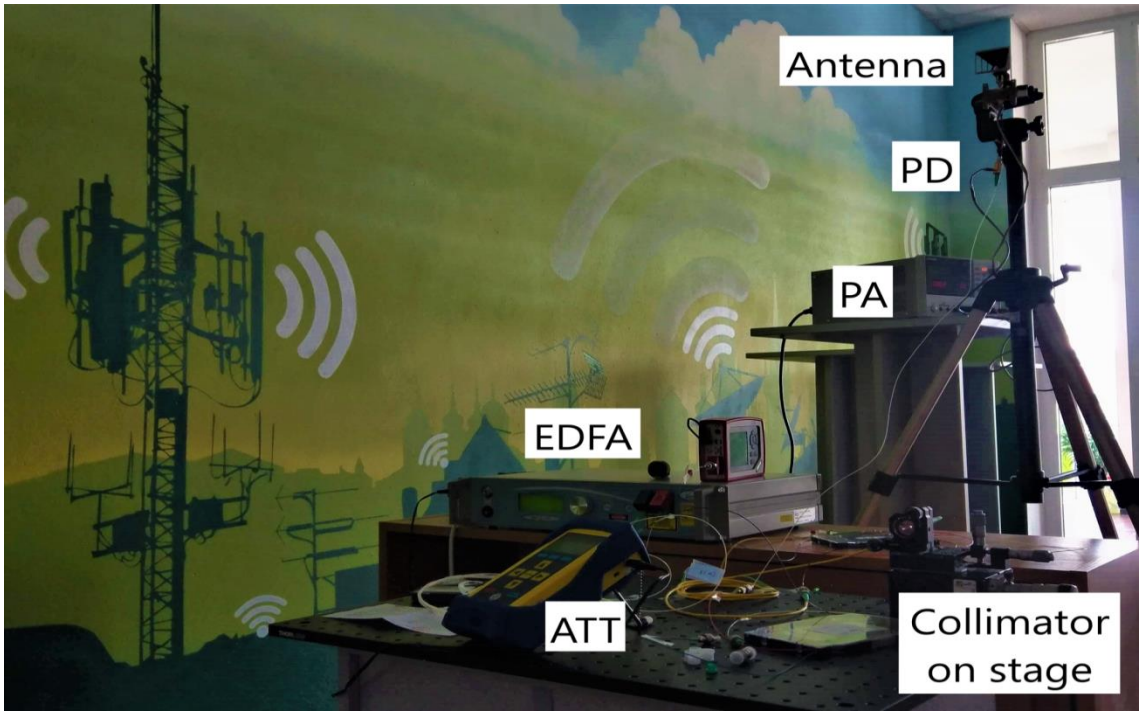

Figure 23 – FSO receiver side for corridor measurement

Now the problem we faced was alignment again. Spot on the detector card for 1550 nm laser beam is visible only up to 3 meters. So we switched to visual fault locator with red laser once again. Because red laser has wavelength around 570 nm, our lens designed for 1550 nm did not collimate light properly and spot size was quickly increasing with distance. After 15 meters, the red spot was so big, it blended with daylight. After some unsuccessful random attempts to receive any sign of signal on the other side of hallway, we almost decided to give up. Luckily at the end of hallway glass door closed and we saw reflection of red light. That was our guidance; we could set up collimator on one side. The other side did have too much light in the window, but when we were walking within 2 meters alongside the propagation path, we could suddenly see high intensity of red light coming from the lenses. By moving our receiving heads left, right, up and down, we could precisely pinpoint where we are aiming, as even when the beam was highly spread, it still had highest intensity at center. With help of others working on the setup, we managed to align our FSO link. As we had no way how to establish controlled turbulence, we measured this scheme without it. It was still very interesting to see how highly the link was affected just by people standing next to the cupboard holding our collimators and would be worsen by up to 2 dB.

8 Results

This section consists of results from measurements for each section as described in previous topic Measurements. All graphs were created using MATLAB R2017b. Results were compared to BER and Error Vector Magnitude limit (EVM) [28] of corresponding transmission and modulation types. For continuous optical wave with On-Off Keying NRZ modulation, BER of 10^{-5} is considered as general limit without forward error correction. For radio modulation and LTE-A model, limits are 17.5 %, 12.5% and 8 % for 4-QAM, 16-QAM and 64-QAM respectively as written in 3GPP TS 36.104 [29].

8.1 Continuous wave transmission

In other work [26], similar setup (laser output at 4.8 dbm @1549 nm) with different collimation system was used: they used fixed graded-index and plano-convex lenses. They have managed to achieve 12 dB losses over the FSO channel. We measured on power meter at receiver side value of 1.87 dBm with system input power level of 6 dBm @1550 nm. This corresponds to 4.13 dB losses including 5 connectors. This meant pretty big accomplishment for start and open doors for further measurements.

8.2 Turbulence influence on part of FSO

Measured Bit error rate during turbulence was zero at start of measurement. After inducing of turbulence, still no error occurred, that is why attenuator had to be installed among the link. With 6 dB attenuation, first errors appeared only during strong turbulences of $C_n^2 \geq 10^{-14}\ \mathrm{m}^{-\frac{2}{3}}$. Trying to increase attenuation resulted in way too low received power on BER tester.

Figure 24 shows results equivalent to extreme turbulence levels, which are breaking the 10^{-5} BER limit for turbulences higher than $C_n^2 \geq 2 \times 10^{-12}\ \mathrm{m}^{-\frac{2}{3}}$. We can also see that the increasing function is not exponential as we expected. Main errors creating these imperfections are caused by computing of refractive index structure parameter itself. We are doing an average of temperature differences, meaning that we don't take into account, that if turbulence is strong on transceiver side, it has have much higher effect, than if it would be on receiver side. Only thing we can confirm is that 2 meters of FSO without addi-

tional attenuation is not enough to make actual damage to OOK NRZ modulated continuous wave signal used in our setup.

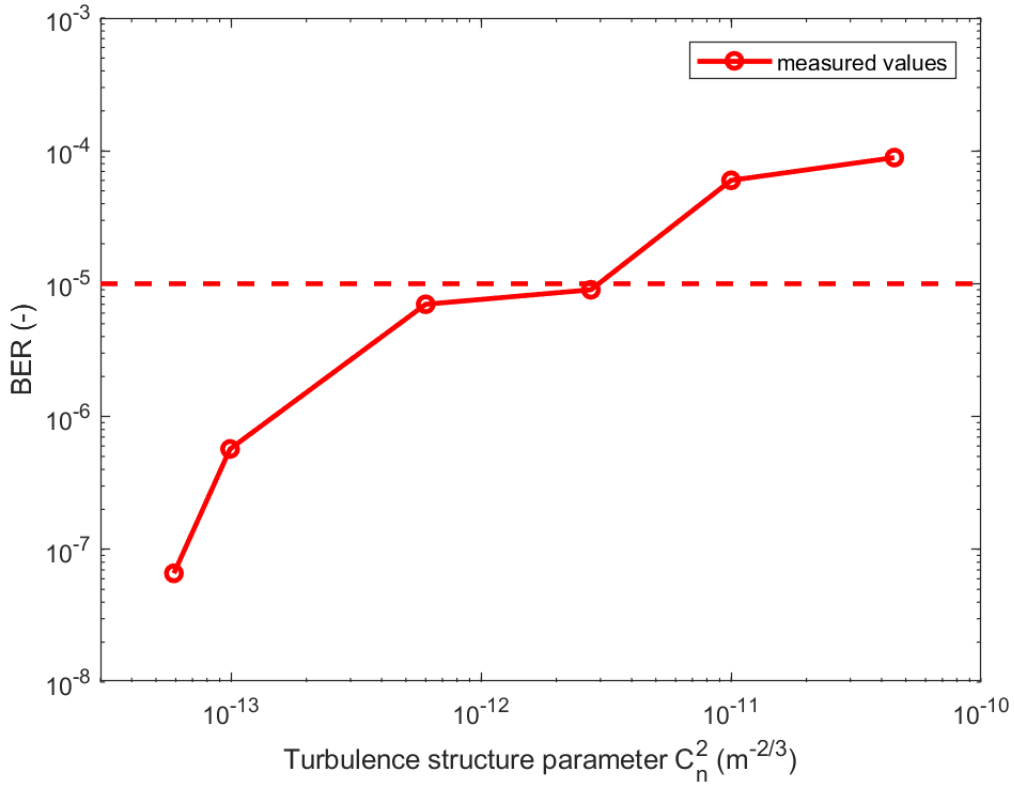

Figure 24 – Measured BER values during strong turbulence

8.3 RoFSO laboratory tests

During this part of experiments, we tested the whole setup under three different turbulences with 5 km of optical fiber. FSO channel alone had 12.5 dB losses. Following figures show dependencies of EVM on received power for three different modulations: 4-QAM, 16-QAM and 64-QAM; and three different turbulences: weak, moderate and strong ($C_n^2 \approx 10^{-16},\ 10^{-14}\ and\ 10^{-13}\ \mathrm{m}^{-\frac{2}{3}}$). Model used for signal generation was LTE-A. Both the EVM and power is analyzed on microwave wave signal received on R&S FSW after going through the whole system. Colored horizontal lines in the figures correspond to EVM limits of each modulation of the same color.

In Figure 25, we can see our first results for weak turbulence ($C_n^2 \approx 10^{-16}\ \mathrm{m}^{-\frac{2}{3}}$). The limits are broken for each modulation almost on same received power level -51 dBm ±1 dB, where higher modulations are reaching it slightly faster by less than

0.5 dB. We can also see that the function is not linear and is slowly increasing EVM the lower the power we receive.

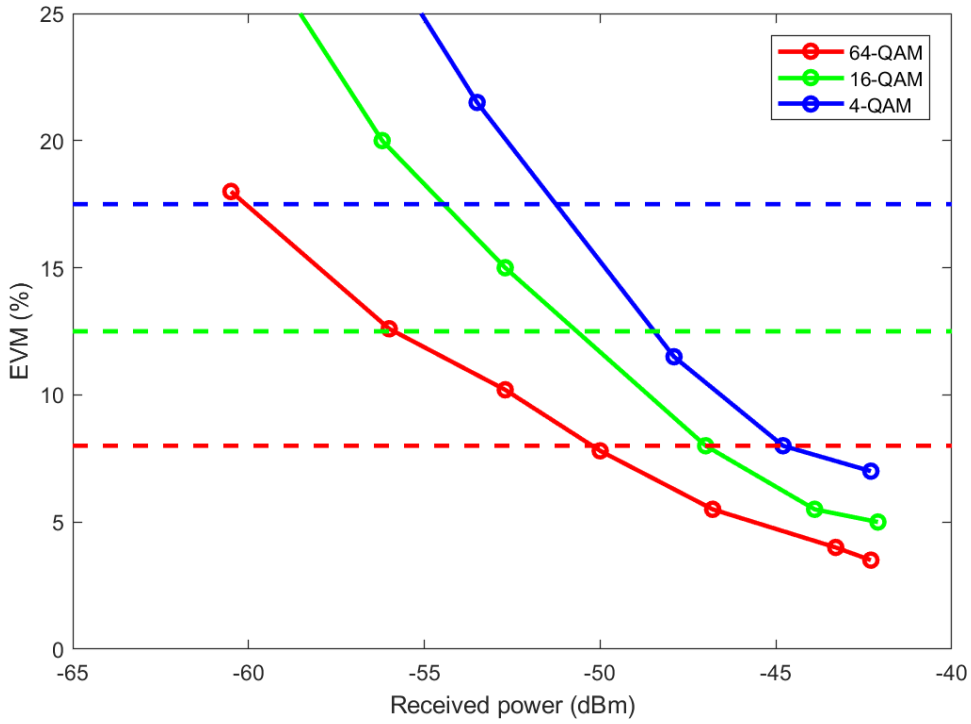

Figure 25 – EVM to received power dependency for weak turbulence

Following measurement was with $C_n^2 \approx 10^{-14}\,\mathrm{m}^{-\frac{2}{3}}$, meaning moderate turbulence. We can see our results in Figure 26. Both 4-QAM and 16-QAM had same results as from weak turbulence levels, where 64-QAM is starting to degrade and increasing the need for received power up to -49 dBm to fulfill the EVM limits.

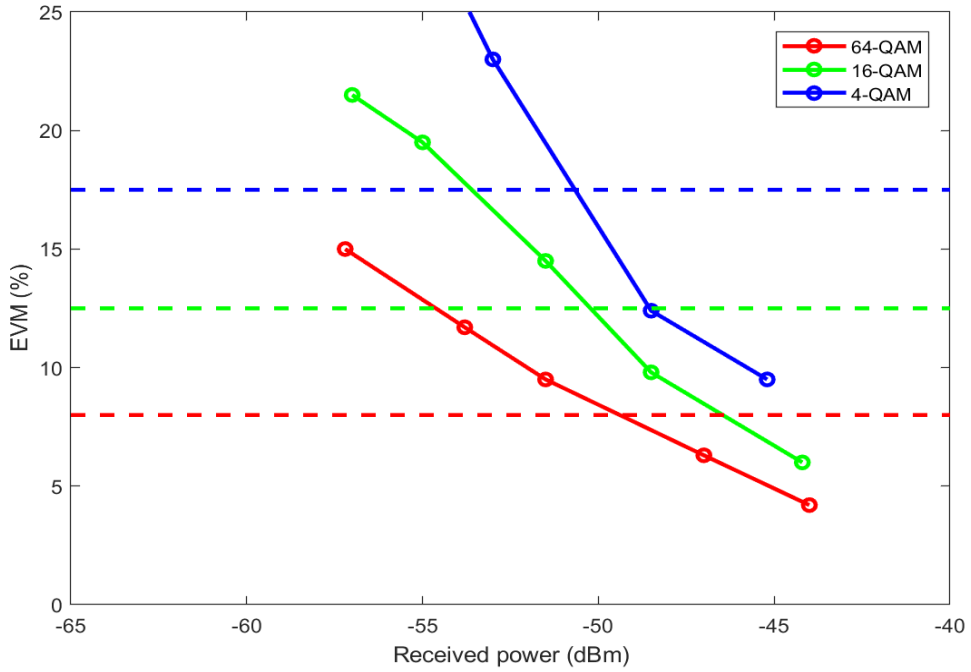

Figure 26 - EVM to received power dependency for moderate turbulence

Last turbulence level was strong with $C_n^2 \approx 10^{-13}\ \mathrm{m}^{-\frac{2}{3}}$. Just by watching the constellation diagrams on our signal and spectrum analyzer, we could see significant amplitude oscillations, making reading of values significantly harder than in previous cases. We can see oscillation minimum on left and extreme maximum on right in Figure 27.

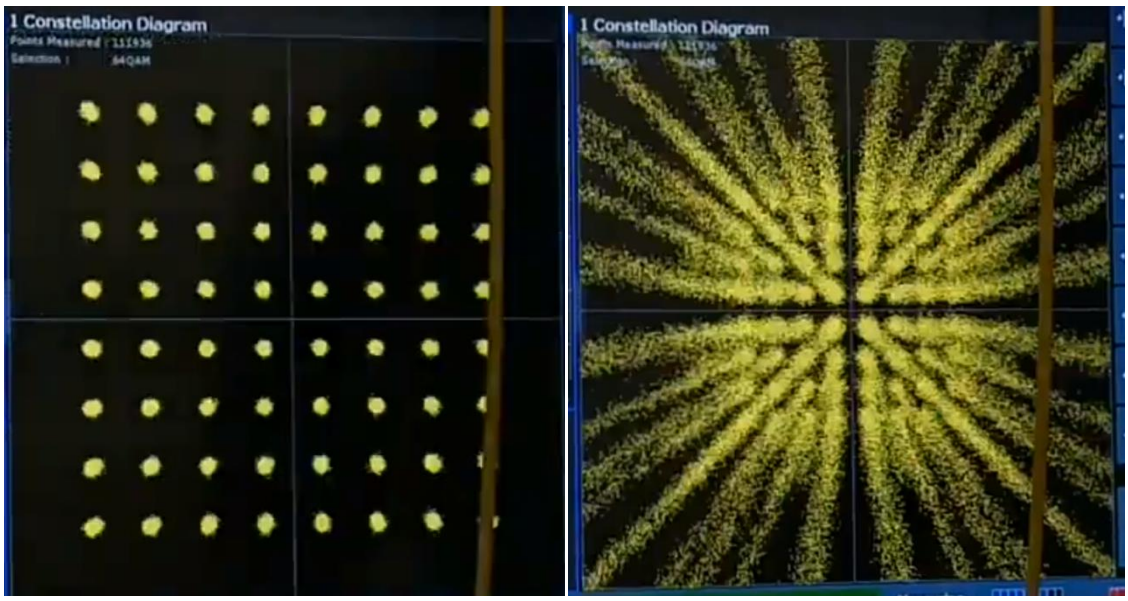

Figure 27 – Constellation diagram oscillations

In Figure 28 we can see, that not even 4-QAM is holding and all modulations increased the need for received power by 3-4 dB. Namely: 4-QAM reached the limit at -47 dBm; 16-QAM at -46.5 dBm; and 64-QAM at -45 dBm.

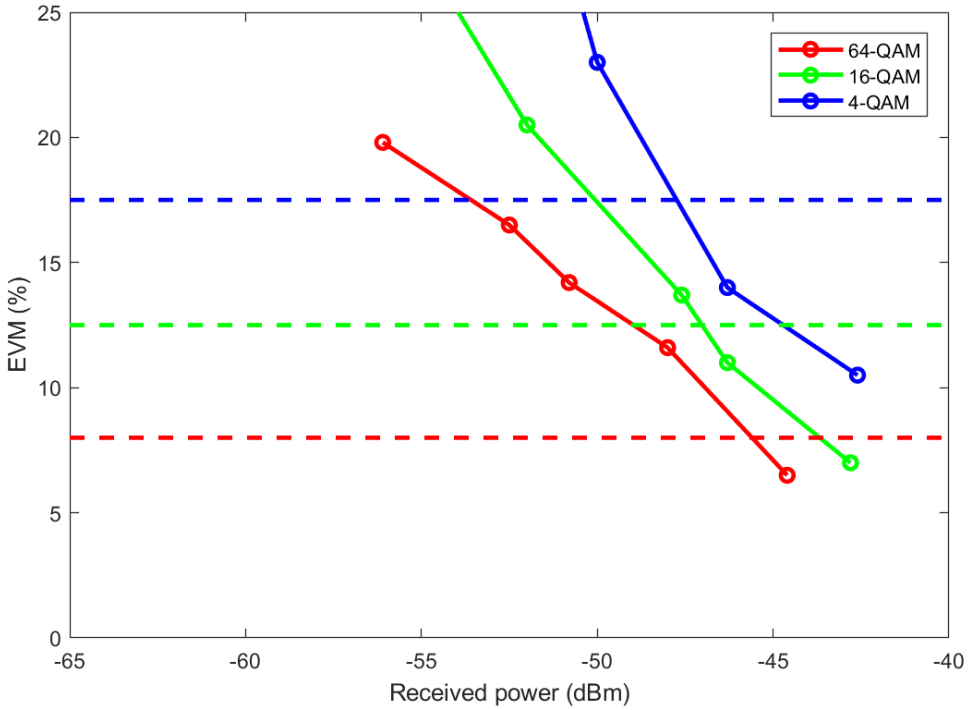

Figure 28 - EVM to received power dependency for strong turbulence

It must be noted, that for strong turbulence, we cannot take the slope and course of function too seriously, as value reading was not very accurate due to very high amplitude oscillations.

8.4 Long RoFSO test in corridor

Last measurement was performed to test how well the transmission performs with higher distance between transmitter and receiver with no turbulence. Compared to previous measurement, we could accurately read all values as no amplitude oscillations were happening. We made measurement for 2 different lengths of optical fiber before the FSO link. Figures show EVM limits for different modulations in relation to Signal to Noise Ratio (SNR).

Results from 5 km one can be seen in Figure 29. EVM limits were reached at SNR 22.5 dB, 24 dB and 27 dB for 4-QAM, 16-QAM and 64-QAM respectively. When we compare these to the same link with additional 45 km of optical fiber, we determine the limits at SNR 22 dB, 22.5 dB and 26dB as seen in Figure 30. We had inaccuracies such as vibrations, people walking around slightly slanting the floor, which either made FSO link better or worse. This was confirmed when we tried to stand on different spots and received power would change by 1-2 dB. It is also worth noting, that we were unable to make as small angle alignments changes as we wanted, so pointing error of approximately 2 dB was present.

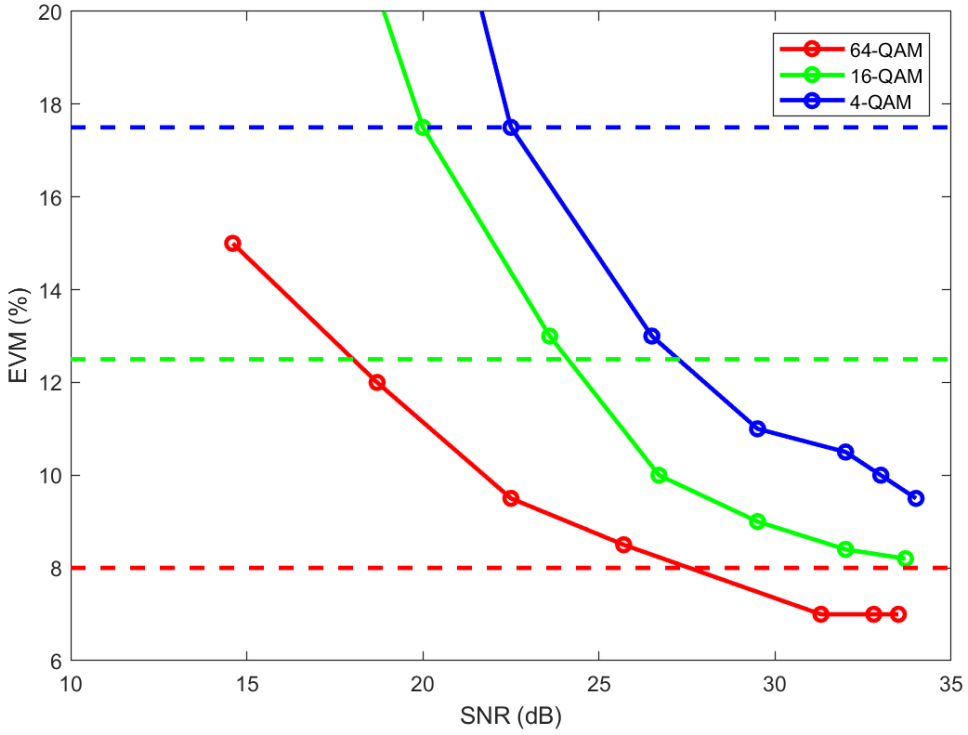

Figure 29 - EVM on SNR dependence for RoFSO with 5 km of optical fiber

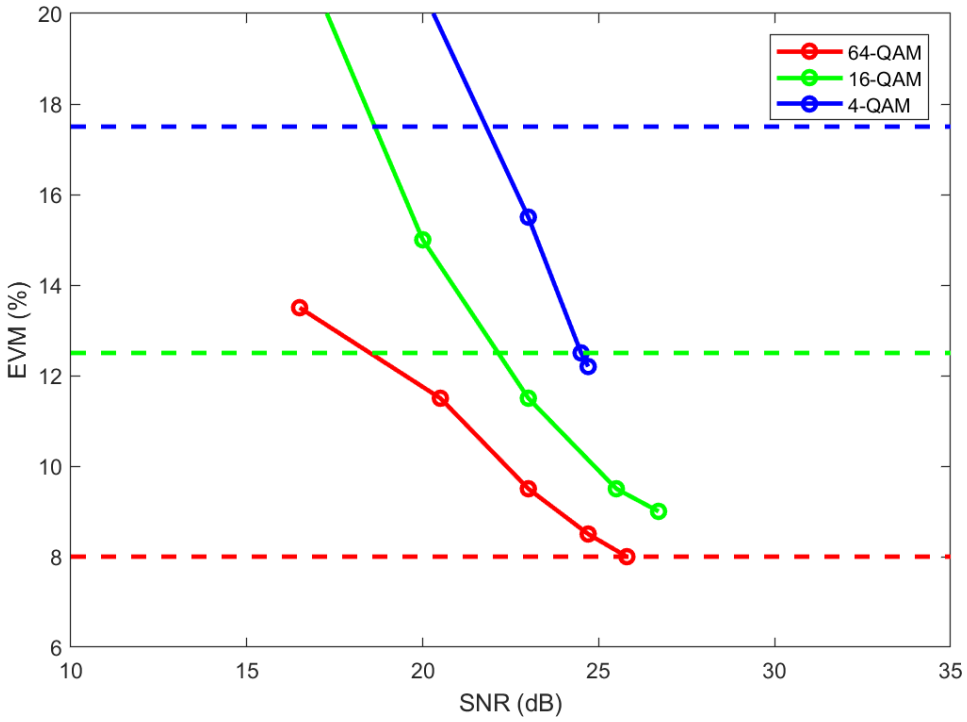

Figure 30 - EVM on SNR dependence for RoFSO with 50 km of fiber

From these numbers, we can design margin for turbulence signal fade to keep EVM under the needed limit. It also shows that even in non turbulent area, effects such as floor slanting, vibrations and pointing errors can play huge role in FSO designs.

9 Conclusion

FSO channels are highly affected by atmospheric phenomena. If we leave out various water vapors, then the highest impact on this link has thermal scintillations creating effects such as beam wandering and angle of arrival error. Due to narrow optical beam, pointing error has to be taken into account when designing communication links and active tracking is needed for longer links and links with either side being on the move. Apart from these disadvantages, FSO offers high data rates, secure unlicensed links [30] and affordable way how to implement them into existing systems and extending the possibilities of both optical fiber communications and wireless RF networks by modulating microwave signal on optical carrier.

We simulated pointing error dependency on received power. Result is exponentially decreasing power with increasing pointing error almost reaching 1 dB for 40 meter link. This can be partially suppressed by increasing the size of lenses or by active tracking. We confirmed that for longer FSO links the turbulence losses are higher.

In experiments we first created 2 m point-to-point continuous wave link with lower losses than what achieved in other article [26]. Main reason was the usage of more advanced collimators, with bigger lens diameter, which partly confirms our first simulation.

We built two meters long turbulence chamber, where we tested both continuous wave and microwave modulated optical carrier signal on turbulence effects.

More results were provided for the complex RoFSO link simulating last mile access system. We tested during weak, moderate and strong turbulences on LTE-A model for three different modulations: 4-QAM, 16-QAM and 64-QAM. While testing under weak and moderate turbulence, all three modulations had similar level, when they reached EVM limits. Under strong turbulence all three modulations needed 3-4 dB increased power to fulfill EVM limits and strong amplitude fades were observed.

Last experiment was performed with the 40 meter RoFSO link. Pointing error was clearly a huge problem and aligning our link proved to be quite difficult. Results consisting of dependency of SNR on EVM can be used for designing power budget for indoor usage as we measured under no turbulence.

For future work I can recommend experimentally measuring effects of pointing error and designing active tracking device, which could automatically align the link. Measurements under real atmospheric effects such as rain or fog could be beneficial for further research and enhancement of FSO links.

10 List of used literature

[1] L. A. Chernov, "Wave Propagation in a Random Medium", McGraw-Hill, New York 1960.

[2] O. Bouchet, H. Sizun, C. Boisrobert, F. de Fornel, P. Favennec, "Free-Space Optics", ISTE, 2006.

[3] D. K. Borah, D. G. Voelz, "Pointing Error Effects on Free-Space Optical Communication Links in the Presence of Atmospheric Turbulence", in *Journal of Lightwave Technology,* vol. 18, no. 1, 2009.

[4] Recommendation ITU-R P.1622-0, "Prediction methods required for the design of Earth-space systems operating between 20 THz and 375 THz", in *ITU Radiocommunication Sector,* 2003.

[5] Recommendation ITU-R P.1622-2, "Propagation data required for the design of Earth-space systems operating between 20 THz and 375 THz", in *ITU Radiocommunication Sector,* 2015

[6] J. H. Churnside, R. J. Lataitis, "Wander of an optical beam in the turbulent atmosphere", in *Applied Optics*, vol. 29, no. 1, 1990.

[7] A. Mukherjee, S. Kar, V. K. Jain, "Analysis of beam wander effect in high turbulence for FSO communication link", in *IET Communications,* vol.12, no.1, 2018.

[8] J. Vitasek, E. Leitgeb, T. David, J. Latal and S. Hejduk, "Misalignment loss of Free Space Optic link," *2014 16th International Conference on Transparent Optical Networks (ICTON)*, Graz, 2014, pp. 1-5.

[9] S. Muta, T. Tsujimura, K. Izumi, "Laser beam tracking system for active free-space optical communication", in *Proceedings of the 2013 IEEE/SICE International Symposium on System Integration*, 2013.

[10] N. A. M. Nor, Z. Ghassemlooy, J. Bohata, P. Saxena, M. Komanec, S. Zvanovec, M. R. Bhatnagar, M.-A. Khalighi, "10 Gbps all-optical relay-assisted FSO system over a turbulence channel," *2015 4th International Workshop on Optical Wireless Communications (IWOW)*, Istanbul, 2015, pp. 69-72.

[11] J. Bohata, S. Zvanovec, M. M. Abadi and Z. Ghassemlooy, "Channel characterization of a last-mile access radio over combined fibre and free-space optics system," *2015*

[12] J. Bohata, P. Pesek, S. Zvanovec, P. Pesek, T. Korinek, M. Mansour Z. Ghassemlooy, "Experimental verification of long-term evolution radio transmissions over dual-polarization combined fiber and free-space optics optical infrastructures", in *Applied Optics,* vol. 55, no. 8, 2016.

[13] J. Mikołajczyk, D. Szabra, R. Matyszkiel and B. Grochowina, "Possibilities of Using FSO/RF Technology in Military Communication Systems," 2018 New Trends in Signal Processing (NTSP), Demanovska Dolina, 2018, pp. 1-4.

[14] K. Kazaura, K. Wakamori, M. Matsumoto, T. Higashino, K. Tsukamoto, S. Komaki, "RoFSO: A Universal Platform for Convergence of Fiber and Free-Space Optical Communication Networks" in *IEEE Communications Magazine,* Feb. 2010.

[15] A. Kaadan, H. Refai and P. Lopresti, "Spherical FSO receivers for UAV communication: geometric coverage models," in *IEEE Transactions on Aerospace and Electronic Systems*, vol. 52, no. 5, pp. 2157-2167, October 2016.

[16] A. K. Majumdar, "Advanced Free Space Optics (FSO)", Springer, 2015, pp. 75-78.

[17] H. E. Nistazakis, A. N. Stassinakis, H. G. Sandalidis and G. S. Tombras, "QAM and PSK OFDM RoFSO Over *M*-Turbulence Induced Fading Channels," in *IEEE Photonics Journal*, vol. 7, no. 1, pp. 1-11, Feb. 2015, Art no. 7900411.
[18] C. H. Lee, "Microwave Photonics", CRC Press, 2013, pp. 175-196.
[19] Y. Zhao, X. Zheng, H. Wen, H. Zhang, "Simplified optical millimeter-wave generation configuration by frequency quadrupling using two cascaded Mach–Zehnder modulators", in *OPTICS LETTERS*, vol. 34, no. 21, 2009.
[20] H. Zhang, L. Cai, S. Xie, K. Zhang, X. Wu, Z. Dong, "A Novel Radio-Over-Fiber System Based on Carrier Suppressed Frequency Eightfold Millimeter Wave Generation", in *IEEE Photonics Journal*, vol. 9, no. 5, 2017.
[21] S. Zvanovec, J. Perez, Z. Ghassemlooy, S. Rajbhandari, J. Libich, "Route diversity analyses for free-space optical wireless links within turbulent scenarios", in *Optics Express*, vol. 21, no. 6, pp. 7641-7650, 2013.
[22] R. Pernice, A. Andò, M. Cardinale, L. Curcio, S. Stivala, A. Parisi, A. C. Busacca, Z. Ghassemlooy, J. Perez, "Indoor free space optics link under the weak turbulence regime: measurements and model validation," in *IET Communications*, vol. 9, no. 1, pp. 62-70, 2 1 2015.
[23] L. C. Andrews, R. L. Phillips, "Laser beam propagation through random media", SPIE, 2005.
[24] N. A. M. Nor, Z. Ghassemlooy, J. Bohata, P. Saxena, M. Komanec, S. Zvanovec, M. R. Bhatnagar, M.-A. Khalighi, "Experimental Investigation of All-Optical Relay-Assisted 10 Gb/s FSO Link Over the Atmospheric Turbulence Channel," in *Journal of Lightwave Technology*, vol. 35, no. 1, pp. 45-53, 1 Jan.1, 2017.
[25] J. Bohata, P. Pesek, S. Zvanovec, Z. Ghassemlooy, "Extended measurement tests of dual polarization radio over fiber and radio over FSO fronthaul in LTE C-RAN architecture," *2016 IEEE 12th International Conference on Wireless and Mobile Computing, Networking and Communications (WiMob)*, New York, NY, 2016, pp. 1-5.
[26] J. Bohata, M. Komanec, J. Spáčil, S. Zvánovec, Z. Ghassemlooy and R. Slavík, "Hybrid RoF-RoFSO System Using Directly Modulated Laser for 24 – 26 GHz 5G Networks," *2018 11th International Symposium on Communication Systems, Networks & Digital Signal Processing (CSNDSP)*, Budapest, 2018, pp. 1-5.
[27] J. Ma, X. Xint, C. Yut, Q. Zhangt, J. Yu, X. Sang, J. Zengt, "Milimeter-Wave Optical Subcarrier Generation by Using an External Modulator and Optical Carrier Suppression," *2007 9th International Conference on Transparent Optical Networks*, Rome, 2007, pp. 273-276.
[28] F Brendel, "Millimeter-Wave Radio-over-Fiber Links based on Mode-Locked Laser Diodes" KIT Scientific Publishing, 2013, pp. 211-218.
[29] Technical Specification Group Radio Access Network; Base Station (BS) radio transmission and reception, Release 11.2; 3GPP TS 36.104 V11.2 (2012-11).
[30] J. Mikołajczyk, D. Szabra, R. Matyszkiel and B. Grochowina, "Possibilities of Using FSO/RF Technology in Military Communication Systems," *2018 New Trends in Signal Processing (NTSP)*, Demanovska Dolina, 2018, pp. 1-4.

11 List of used Figures